Ionization and charge transfer in He^{2+}–rare-gas collisions. II

R. D. DuBois
Pacific Northwest Laboratory, Richland, Washington 99352
(Received 6 April 1987)

New measurements of absolute cross sections for multiple ionization of helium, neon, argon, and krypton by 50–500-keV/amu He^{2+} impact are presented. By measuring projectile-ion–target-ion coincidences, these cross sections are obtained for the direct ionization as well as the single- and double-electron-capture channels. The present data are combined with previous measurements by the author that covered the energy range between 5 and 67 keV/amu in order to provide a broader description of He^{2+} impact ionization of atomic targets. The earlier measurements were found to require reevaluation in order to correct ion detection efficiencies used in that study. An analysis of the direct-multiple-ionization cross sections demonstrates that a simple impact-parameter, independent-electron model can be used to describe these cross sections over a broad range of low to intermediate impact energies. In particular, this analysis, when applied to fully stripped ion ($1 \leq Z \leq 8$) impact on helium, yields a single universal curve in the velocity range investigated here.

I. INTRODUCTION

In recent years there have been many studies of multiple ionization of atoms resulting from fast charged-particle impact. Although single ionization induced by fast bare-projectile impact is fairly well understood, efforts to understand multiple-ionization phenomena are more difficult. Even in the simplest case, double ionization of helium, McGuire has shown that the double ionization observed for higher impact energies results from a single projectile-target interaction whereas at lower impact energies a two-step (multiple) projectile-target interaction dominates.[1] In an intermediate-energy range where both mechanisms contribute, it was suggested that interference effects may also occur.

Experimentally, Shah and Gilbody[2] and Knudsen *et al.*[3] have studied single and double ionization of helium resulting from bare-ion impact. In heavy targets, which thus far have received little attention, direct ionization and charge transfer involving outer-shell as well as inner-shell target electrons contribute to the total observed multiple-ionization cross sections. Recently, for proton impact on helium, neon, argon, and krypton,[4] these individual cross sections were identified and quantized. It was then shown that the direct multiple outer-shell ionization cross sections are well described by an independent-electron picture (i.e., a multiple interaction model) over a fairly broad energy range.

In the case of bare-helium-ion impact, the author has recently published multiple-ionization cross sections for several atomic targets[5] but only for impact energies up to 67 keV/amu. These measurements have now been extended to 500 keV/amu. As before, coincidences between the postcollision slow target ions and the fast projectile ions have been measured and cross sections for multiple target ionization (σ_q^{2j}) calculated. In this notation the superscripts represent the projectile initial and final charge states and the subscript is the final target charge state. By studying the direct-ionization channel ($j=2$) as well as the single- and double-electron-capture channels ($j=1$ and 0, respectively), a *complete* picture of ionization by He^{2+} impact on He, Ne, Ar, and Kr is obtained. These individual cross sections can then be appropriately combined in order to provide information about total positive-ion and free-electron production as well as total single- and double-electron-capture cross sections.

In addition, these new data can be used to test the independent-electron calculations of Becker *et al.*[6] for neon. Also, it was previously observed that for double-electron capture from argon and krypton targets, the cross sections for capturing two electrons plus ionizing an additional electron were larger than the cross sections for simply capturing two electrons. This was observed to occur for all impact energies investigated indicating that it was not a result of inner-shell capture followed by an Auger relaxation. The present data were originally intended to investigate this phenomenon at higher impact energies, but, as will be shown, fail to confirm these previous observations.

II. EXPERIMENTAL PROCEDURE

Some details of the experimental apparatus and procedure used to obtain the present data will be given since these differ from those previously described in Ref. 5. In general, the data accumulation procedure consisted of directing an energy-analyzed, collimated beam of $^4He^{2+}$ ions through a target cell (diameter of approximately 1 cm, pressure of ≈ 0.1 pascal) and then electrostatically charge-state-analyzing the emerging beam before detecting it with a ceramic channel electron multiplier that was used as a secondary emission detector (see Fig. 1). An electric field was used to extract target ions having charge state q that result from projectile-target interactions in the collision region. These ions traveled through a field-free drift region, after which they were accelerated to a higher energy ($\approx 3kqV$), traveled an additional distance in a field-free region, and were then counted by a channel electron multiplier. Standard coin-

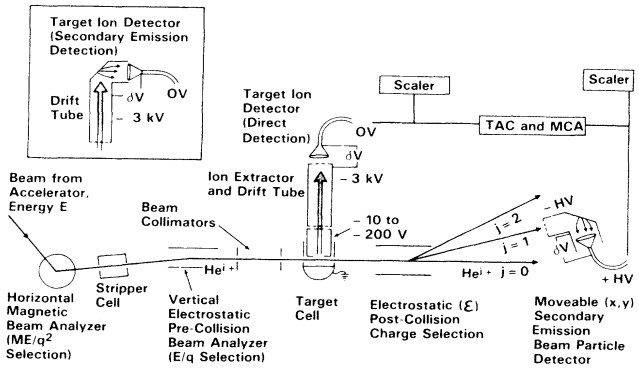

FIG. 1. Schematic of experimental apparatus used to measure multiple ionization of gaseous targets. Inset shows secondary emission target-ion detector.

cidence electronics processed the slow and fast ion signals in order to produce time-of-flight target-ion spectra.

The integrated peak intensities (B_q^{2j}) obtained from these spectra provided information about target ionization resulting from directly ionizing ($j=2$) or electron-capturing ($j=1$ or 0) collisions depending upon the particular projectile charge state selected as one of the coincidence partners. These peak intensities were converted into absolute cross sections (σ_q^{2j}) for multiple target ionization by normalizing to the total positive-ion-production cross sections of Itoh and Rudd.[7] In addition, the individual σ_q^{2j} cross sections can be summed in various combinations to yield total free-electron production (σ_-), single- (σ^{21}), and double- (σ^{20}) electron-capture cross sections as will be shown below. Several experimental details specific to the present work will now be discussed.

A. $^4He^{2+}$ production

An uncontaminated $^4He^{2+}$ beam was produced by a combination of horizontal magnetic field and vertical electric field separation (see Fig. 1). Initially, $^4He^+$ ions of energy E were selected by the magnetic field after which they were passed through a stripper cell. The $^4He^{2+}$ component formed in the cell was then selected using the electric field. However, it was found that an O^{2+} contaminant was also present. This was attributed to O^+ ions originating in the ion source that were also accelerated to energy E. Before entering the analyzing magnet a small percentage of these ions stripped to O^{2+} due to interactions with the residual gas, thus allowing them to be selected along with the $^4He^+$ ions since both meet the same ME/q^2 conditions for magnetic selection. The electric field then selected both the O^{2+} and He^{2+} ions since both met the same E/q requirements. Thus, in order to obtain a clean $^4He^{2+}$ beam this pre-magnetic-field stripping was exploited. In this case $^4He^+$ ions were accelerated to energy E and the small percentage of them that prestripped to $^4He^{2+}$ were selected by the analyzing magnet. Now, however, the magnetic field also selected any H^+ ions that were present. The H^+ ions were then rejected by the electric field thus producing an uncontaminated $^4He^{2+}$ beam.

B. Projectile-ion detection

The projectile ions were detected using a single detector that could be centered on the particular beam component of interest. The efficiency of this detector (η_b), when used to count the secondary electron emission from a brass plate, was measured at high impact energies by alternately directing a weak beam onto it and onto a surface barrier detector for which unit efficiency was assumed. Such measurements yielded values of 0.78 ± 0.05 for He^+ ions and 0.84 ± 0.04 for neutral-helium impact. (No measurements for He^{2+} ions were made.) These values are in reasonable agreement with those values obtained by taking the ratio of the total target-ion coincidence rate to the total noncoincidence target-ion rate yielding 0.68 ± 0.07 for He^{2+} impact and 0.70 ± 0.07 for He^+ impact. These tend to imply near-unit detection efficiency for the fast ion detector since a 85% transparent grid covers the entrance to this detector. Any discrepancy between these measured efficiencies and 0.85 is not attributed to solid angle limitations since measurements made using the secondary emission detector ($\Delta\Omega$ either 2 or 4 mrad) and the surface barrier detector ($\Delta\Omega\approx16$ mrad) gave similar results.

C. Recoil-ion detection

The efficiencies for detecting the slow recoil ions were investigated in considerable detail since some inconsistencies were found between cross sections measured using the present apparatus with those measured earlier in our laboratory[5] and also with various total cross sections (see Ref. 5). During this investigation and data collection, three different recoil-ion detection systems were used. Initially, a 10-V/cm extraction field and a 3.5-cm-long flight path filled with target gas were used. In the first system, the recoil-ion channel electron multiplier was positioned to count the secondary electron emission from a brass surface (see inset in Fig. 1). The second system moved the channel electron multiplier to directly detect the recoil ions although the flight tube remained the same (see Fig. 1). The final system used a 400-V/cm extraction field, a 5.5-cm flight path with several pumping holes in order to reduce the gas density throughout the flight path, and the detector positioned to directly detect the recoil ions. For each configuration B_q^{21} ($q=1-4$ or 5) was measured for a fixed integrated beam charge multiplied by target gas pressure and was found to be independent of extraction field and target pressure for values ranging between approximately half to double the values quoted.

The efficiency for detecting recoil ions of various charge states [$\eta(q)$] was obtained by measuring B_q^{21} for various voltages V of the final drift tube (500–3500 V) and hence for various recoil-ion energies qV. In the previous study[5] this type of data for recoil argon ions was interpreted as an indication of a charge-independent detection efficiency for ion energies above approximately 2 keV. However, the present data obtained for higher

charge states and with better statistics show that the detection efficiency depends on the velocity with which these slow ions impact the detector. The relative intensities of B_q^{21} for various recoil-ion energies and target-ion species, plotted versus their velocities, were found to lie on a universal curve for the secondary emission detector originally used [see Fig. 2(a)]. In the later configuration where the ions directly impinge upon the detector cone, a different situation exists. In this case [Fig. 2(b)], only for velocities exceeding approximately 0.6 $(\text{keV/amu})^{1/2}$ does a universal curve exist. Note that in this case, geometrical as well as absolute beam charge and target density information were used to place these recoil-ion detection efficiencies on an absolute scale.

In both cases it was found that the detection efficiencies depended upon the recoil-ion mass and energy. This is in contrast to the study done by Fricke *et al.*[8] The reason for this is not clear. It does not appear that any lensing action was affecting the present investigation since equivalent results were obtained for extraction fields of 20 and 400 V/cm which would result in entirely different focusing effects.

Using this new information, the recoil-ion detection efficiency data from Ref. 5 was reanalyzed. It was found that these data are in agreement with the results shown in Fig. 2(a) and it is concluded that the cross sections presented in Refs. 5 and 9–11 need to be adjusted to account for this error. Recommended adjustments for these data are given in the Appendix while the cross sections presented in Ref. 5 have been recalculated and are included with the present data.

After investigating these experimental parameters, the cross-section data were collected in the following manner. Time-of-flight recoil-ion spectra were measured for known target-gas pressures (generally 0.1 pascal) and integrated beam currents. First no postcollision projectile charge state separation was used ($\varepsilon=0$ in Fig. 1). Thus total multiple ionization intensities ($B_q^T=\sum B_q^{2j}$) were measured. Then the electric field was turned on and the fast ion detector was sequentially centered on the He^{2+} (for direct ionization), the He^+ (for single-electron capture), and finally on the He^0 (for double-electron capture) components. In each case the target ionization charge state intensities (B_q^{2j}) were recorded for known target-gas pressures and beam charge. Since the total beam intensity could not be monitored in all cases, this normalization was done by normalizing to the *total noncoincidence* recoil-ion intensity. The results were found to be internally consistent to within 10% (i.e., $B_q^T \approx \sum B_q^{2j}$).

These raw intensities are related to the absolute cross sections by

$$\sigma_q^{2j}=\frac{B_q^{2j}/\eta(q)}{(I/\eta_b)NlT} ,$$

where $\eta(q)$ is the recoil-ion detection efficiency, η_b is the fast ion detection efficiency, I is the integrated beam intensity, N is the target-gas density, l is the interaction length, and T is the optical transmission of the recoil-ion detection system due to the grids used. Normalization to the total positive-ion cross sections (σ_+) of Itoh and Rudd[7] was used at each impact energy to place the recoil-ion detection efficiencies on an absolute scale, i.e.,

$$\sigma_+=\frac{\sum qB_q^T/\eta(q)}{(I/\eta_b)NlT} .$$

This was done by calculating relative values for σ_+ using relative values for $\eta(q)$ and then normalizing to the absolute σ_+ cross section by adjusting $\eta(q)$. It is the average of all these detection efficiencies that is shown in Fig. 2(b).

The individual σ_q^{2j} cross sections were then combined to provide total free-electron-production cross sections

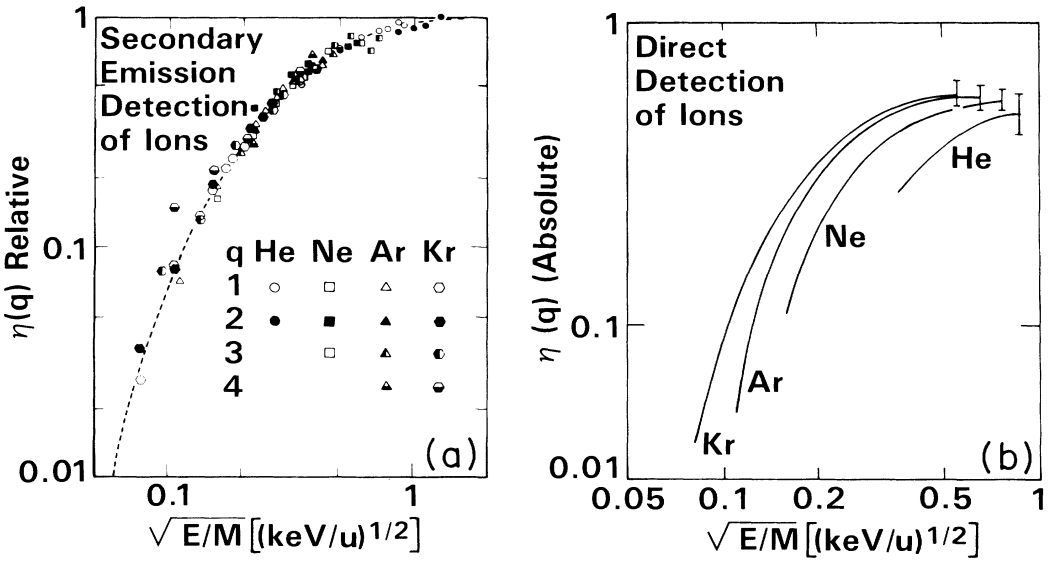

FIG. 2. Detection efficiencies for slow target ions. (a) Relative detection efficiencies for the secondary emission detector shown in inset of Fig. 1. (b) Absolute efficiencies for the direct detection of the various target ions studied.

TABLE I. Absolute cross sections (in units of 10^{-16} cm^2) for He^{2+}-He collisions. σ_q^{2j} $(j=2,1,0)$ are for direct-ionization, single- and double-electron capture, respectively. σ_+, total positive-ion-production cross sections from Ref. 7 used for normalization purposes. σ_-, total free-electron-production cross sections obtained from present σ_q^{2j} cross sections as described in the text. The 5–66.7 keV/u data are recalculated values taken from Ref. 5 as described in the text. Typical uncertainties are ±15% except for those values indicated with asterisks which have 25–30% uncertainties.

	He^{2+}-He							
			Direct ionization		Single capture			Double capture
E/M (keV/u)	σ_+	σ_-	σ_1^{22}	σ_2^{22}	σ^{21}	σ_1^{21}	σ_2^{21}	σ^{20}
5		0.0162			0.49	0.474	0.0162	
10	3.8	0.0320			0.779	0.750	0.0320*	1.49
16.7	5.0	0.206	0.0785		2.13	2.01	0.127	1.33
33.3	6.0	0.574	0.186*		3.17	2.78	0.388	1.13
50	5.6	1.10	0.623	0.0153*	2.96	2.52	0.444	0.768
66.7	5.15	1.52	1.10		2.58	2.16	0.425	0.522
50	5.6	1.32	0.949	0.0219	2.30	1.97	0.330	0.619
75	4.9	2.05	1.66	0.0282*	2.10	1.77	0.330	0.335
100	4.3	2.67	2.35	0.0632	1.17	0.976	0.191	0.135
175	3.1	2.43	2.18	0.0741	0.536	0.437	0.0991	0.108
250	2.4	2.34	2.20	0.0566	0.184	0.154	0.0302	0.001 69
375	1.85	1.73	1.66	0.0303	0.0411	0.0357	0.005 39	
500	1.50	1.45	1.39	0.0286	0.0131	0.0109	0.002 23	

$[\sigma_- = \sum(q+j-2)\sigma_q^{2j}]$ and total single- $(\sigma^{21}=\sum\sigma_q^{21})$ and double- $(\sigma^{20}=\sum\sigma_q^{20}$, for $q\geq 2)$ electron-capture cross sections. In cases where data obtained using the different recoil-ion systems were averaged, generally agreement within 10–15% in absolute magnitude was found. In some cases, most notably for the highest charge states measured, larger errors exist.

The data presented in the following section consist of the present measurements for $^4He^{2+}$ impact energies ranging from 200 to 2000 keV and the recalculated $^3He^{2+}$ between 15 and 200 keV that were originally published in Ref. 5. The recalculation includes adjustments

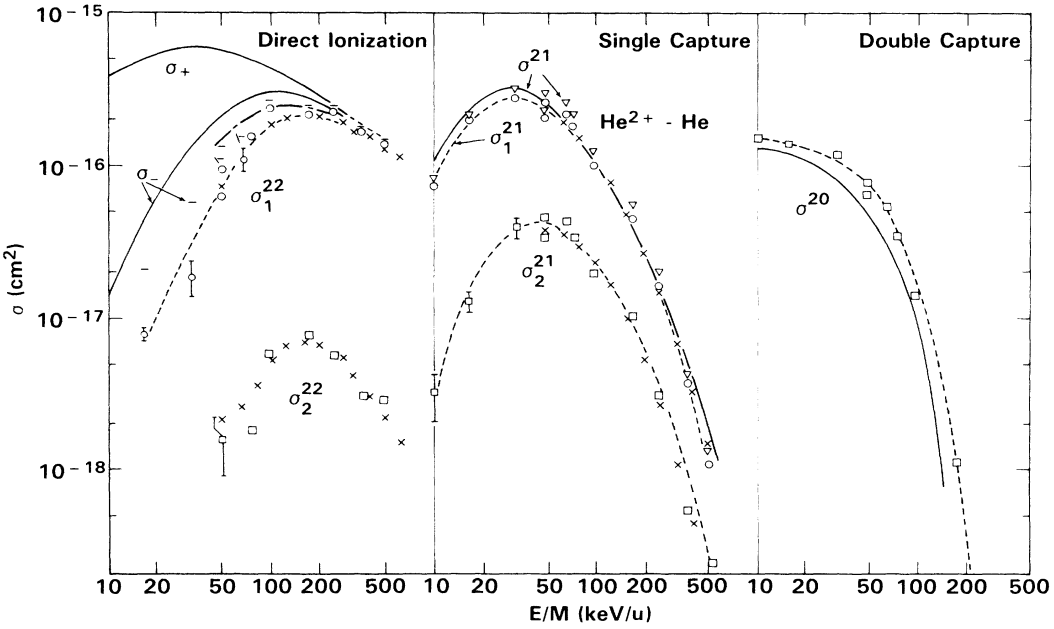

FIG. 3. Absolute cross sections for multiple ionization of helium by He^{2+} impact. σ_+: ——, total positive-charge-production cross sections from Ref. 7 used for normalization. Dashed curve is extrapolation to higher energies. σ_-: ——, total free-electron-production cross section, Ref. 7; – – –, Ref. 12; —, present work. σ^{21} and σ^{20}: ——, total single- and double-capture cross sections from Refs. 7, 13, and 15; ▽ (single) and □ (double), present work. σ_q^{2j}: ○,□, present work; ×, Ref. 2. Error bars, where shown, represent repeat measurements. Dashed curves are only to guide the eye.

made using new information about $\eta(q)$ and an renormalization to σ_+ since it was found that normalization to σ^{21} at low impact energies was inconsistent with normalization to σ_+ which was used for the higher impact energies.

III. RESULTS AND DISCUSSION

The cross-section data will be presented in tabular form in order to facilitate its use. Only for helium and neon targets will graphical representations be presented but these serve as representative examples of the present data. Following the presentation of the data, a brief analysis of the direct-multiple-ionization cross sections for the helium and neon targets will be given.

A. Helium

Cross sections for single and double ionization of helium due to direct ionization as well as single and double electron capture by 5–500 keV/amu He^{2+} impact are tabulated in Table I and shown in Fig. 3. These individual σ_q^{2j} cross sections have been appropriately summed to provide information about the total free-electron-production (σ_-) and single-electron-capture (σ^{21}) cross sections. The data are considered to have uncertainties of 10–15% except for those cases where larger uncertainties are indicated.

Included in Fig. 3 are the σ_+ and σ_- measurements of Itoh and Rudd[7] and Puckett *et al.*[12] as well as total single- and double-capture cross sections.[7,13] In addition the σ_q^{2j} measurements of Shah and Gilbody,[2] which are seen to be in total agreement with the present data, are shown. The present data are in better agreement with the σ_- measurements of Puckett *et al.* than with those of Itoh and Rudd. In the case of electron capture, the present data tend to be larger by 20–40% than the values taken from the literature. Although the situation for double capture is not clear, the σ_q^{2j} data of Shah and Gilbody tend to support the present σ^{21} and σ_- cross sections.

B. Neon

Data for multiple ionization of neon are presented in Fig. 4 and Table II. As can be seen, single ionization of neon dominates the direct-ionization channel and pure capture always is the most important process in both the single- and double-capture channels. However, capture plus an additional ionization plays a significant role for the higher impact energies. Also included in Fig. 4 are the total cross-section measurements of Itoh and Rudd which are the only other measurements of which the author is aware. The present data, which were normalized to their σ_+ measurements, indicates an increasingly smaller σ_- cross section as the impact energy is decreased. Considering that the present experiment is unaffected by spurious secondary electron signals and beam neutralization at low impact energies, unlike the situation for the total yield measurements,[14] and considering the reasonably good agreement demonstrated in the total-electron-capture channels, the present data are

TABLE II. Absolute cross sections (in units of 10^{-16} cm^2) for He^{2+}-Ne collisions. Notation and uncertainties are as given for Table I.

			He^{2+}-Ne												
			Direct ionization				Single capture				Double capture				
E/M (keV/u)	σ_+	σ_-	σ_1^{22}	σ_2^{22}	σ_3^{22}	σ_4^{22}	σ^{21}	σ_1^{21}	σ_2^{21}	σ_3^{21}	σ_4^{21}	σ^{20}	σ_2^{20}	σ_3^{20}	σ_4^{20}
5	7	0.117					3.53	3.44	0.0979			1.67	1.66	0.0195	
10	9.6	0.611					4.49	3.94	0.548			2.25	2.18	0.0633	
16.7	10.1	1.20	0.0882				5.00	4.12	0.834	0.0467*	0.00148	1.96	1.79	0.168	0.00334
33.3	9.7	2.31	0.615	0.0588	0.00556		4.87	3.65	1.09	0.132	0.0024	1.26	1.07	0.185	0.0074*
50	9.0	3.39	1.21	0.0942*	0.0178*	0.0029	3.87	2.38	1.24	0.237	0.0149	0.868	0.681	0.178	0.0092
66.7	8.5	3.75	1.53	0.128	0.0421		3.47	2.11	1.10	0.255	0.168*	0.635	0.460	0.164	0.0111
50	9.0	3.08	1.64	0.112	0.0147		3.25	2.34	0.772	0.133	0.00253	0.656	0.538	0.112	0.00570
75	8.2	3.95	1.97	0.140	0.040	0.00719	3.15	1.99	0.918	0.226	0.0149	0.494	0.371	0.115	0.00915*
100	7.4	4.52	2.48	0.209	0.0535	0.00693*	2.33	1.32	0.752	0.234	0.0234	0.363	0.245	0.104	0.0130
175	6.1	4.59	2.77	0.342	0.0666	0.0066	1.42	0.737	0.509	0.152	0.0189	0.0915	0.0573	0.0301	0.00398*
250	5.3	4.38	2.85	0.396	0.0675	0.00674	0.798	0.410	0.289	0.0886	0.0108	0.0241	0.0160	0.00683	0.00126
375	4.6	4.22	3.02	0.408	0.0645	0.0047*	0.318*	0.186	0.0968*	0.0315	0.00325	0.00716	0.00567*	0.00104	0.00042
500	4.1	4.07	3.10	0.362	0.0486	0.00668*	0.120	0.0613	0.0452	0.0120	0.00127	0.00172	0.00140	0.000269	0.000053

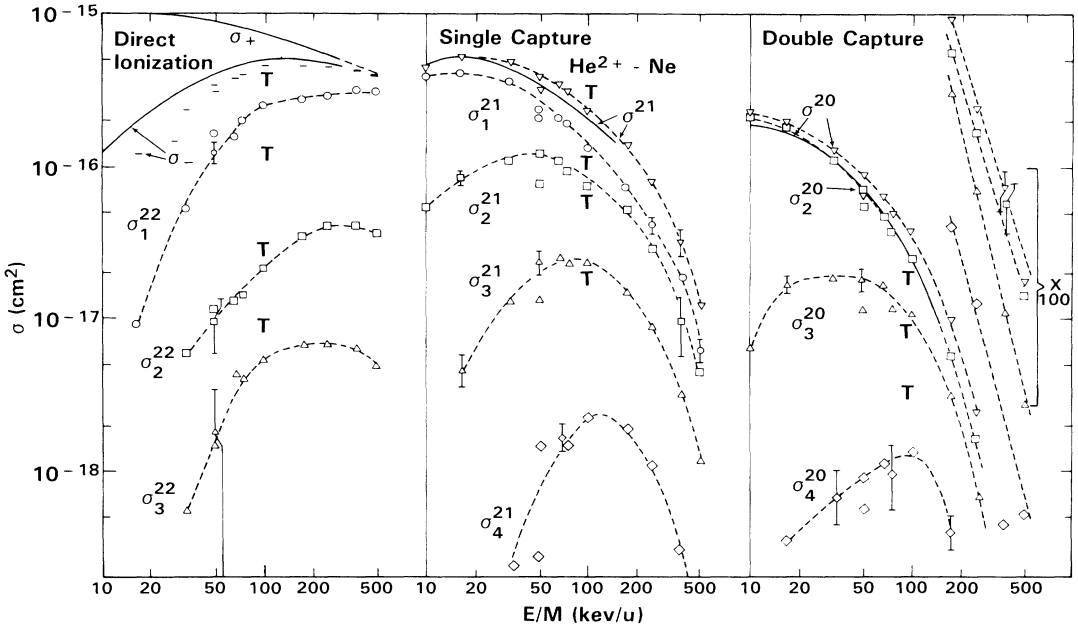

FIG. 4. Cross sections for multiple ionization of neon by He^{2+} impact. σ_+: ——, total positive charge production from Ref. 7 used for normalization. Dashed portion is extrapolation to higher energies. σ_-: total free-electron-production cross sections: ——, Ref. 7; —, present work; T, calculations from Ref. 6. σ^{21} and σ^{20}: total single- and double-capture cross sections: ——, Ref. 7; ▽, present work; T, calculation from Ref. 6. σ_q^{2j}: ○,□,△,◇, present work; T, calculated values from Ref. 6. Note that the calculated σ_q^{20} values have been normalized to the experimental σ^{20} value. Error bars and dashed curves are as described in Fig. 3 caption.

considered to be more accurate. We find that the present total-capture cross sections tend to be slightly larger ($\approx$20%) than those of Itoh and Rudd although having the same energy dependence. This indicates an inconsistency between the σ_+ and the capture cross sections presented in Ref. 7.

A comparison with the independent Fermi particle model calculations of Becker *et al.*[6] shows that the theory determines the charge state distribution quite well in the case of single electron capture but less well in the double-capture and direct-ionization cases. Although 100 keV/amu is a rather low impact energy for testing the theory, preliminary calculations at higher impact energies have given similar comparisons.

C. Argon and krypton

Data for argon and krypton are presented in Tables III and IV, respectively. Multiple ionization is becoming relatively more important and competitive with respect to single ionization. However, the only indication of higher degrees of ionization being larger than lower degrees of ionization occurs at the highest impact energies where inner-shell ionization is becoming important. Due to the present recoil-ion detection efficiencies which differ from those used previously, the new data do not indicate that double capture plus an additional ionization is larger than double capture alone as was previously found. The new and old data[5] are in complete agreement except for the case of pure double capture (σ_2^{20}) from krypton. Even after correcting for the detection efficiencies, the earlier data is inconsistent with the present values. No explanation for this can be given although the present data are assumed to be correct. Unfortunately, the earlier data cannot be rechecked as the apparatus no longer exists.

For both argon and krypton, the present σ_- cross sections are smaller at lower impact energies than those measured by Itoh and Rudd[7] and by Puckett *et al.*[12] Again the present total-capture cross sections are slightly larger than those of Itoh and Rudd, but tend to agree with other previously measured values.[15]

IV. DIRECT-MULTIPLE-IONIZATION ANALYSIS

Following a procedure that was recently used to analyze multiple outer-shell ionization of atoms resulting from proton impact,[4] it is possible to obtain some information about the interaction mechanism(s) leading to the direct-ionization cross sections that have just been presented. This is done by studying the ratios of direct-multiple- to direct-single-ionization cross sections. For example, the projectile can be assumed to interact once with a single target electron and this electron can in turn interact with other target electrons such that all are ejected. This interaction is clearly first order in the projectile-target interaction. Hence one would expect that the first- and higher-order direct-ionization cross sections should have roughly the same energy dependences, e.g., that the ratio of direct double to direct sin-

TABLE III. Absolute cross sections (in units of 10^{-16} cm^2) for He^{2+}-Ar collisions. Notation and uncertainties are as given for Table I.

	He^{2+}-Ar																			
E/M	Direct ionization								Single capture							Double capture				
(keV/u)	σ_+	σ_-	σ_1^{22}	σ_2^{22}	σ_3^{22}	σ_4^{22}	σ_5^{22}	σ_6^{22}	σ^{21}	σ_1^{21}	σ_2^{21}	σ_3^{21}	σ_4^{21}	σ_5^{21}	σ_6^{21}	σ^{20}	σ_2^{20}	σ_3^{20}	σ_4^{20}	σ_5^{20}
5	18.2	2.72							10.8	9.19	1.53	0.0910				2.31	1.30	0.991	0.0130	
10	24	4.20	0.187	0.0336					13.8	11.7	1.74	0.369	0.006 26*			2.99	1.61*	1.30	0.0770	
16.7	26.4	6.04	0.638	0.104	0.0228				14.5	11.7	2.04	0.687	0.0477			2.94	1.52*	1.27	0.149	
33.3	25.2	10.1	3.08	0.317	0.107	0.0044			11.4	7.86	2.35	1.05	0.136	0.0119		1.88	0.895	0.847	0.133*	0.006 48
50	24.0	12.9	5.18	0.634	0.260*	0.0299			8.81	5.29	2.26	1.05	0.176	0.0121		1.12	0.534	0.499	0.0841	0.001 79
66.7	21.9	14.2	6.28	0.872	0.324*	0.0586*			6.43	3.58	2.14	0.944	0.161*	0.0089*		0.665	0.325	0.286	0.0509*	0.004 72*
50	24.0	12.4	5.30	0.682	0.221	0.0411			7.86*	4.81*	1.97	0.917	0.157			1.40	0.846	0.477	0.0802	0.003 2*
75	21.0	14.6	6.77	0.960	0.287	0.0463	0.003 95		6.51*	3.35*	2.05	0.951	0.146	0.0134	0.005 23	0.591	0.308	0.236	0.0415	0.005 18*
100	19.0	14.2	7.02	1.27	0.370*	0.0419*	0.002 28		4.41	2.08	1.58	0.642	0.0953	0.009 97*		0.189	0.103	0.0847*	0.0184*	0.002 0*
175	14.3	11.6	6.84	1.43	0.293	0.0324	0.005 59		1.08	0.475	0.408	0.155	0.0312	0.007 33	0.001 85					
250	12.6	13.1	8.87	1.50	0.242	0.0239	0.006 39	0.003 56	0.413*	0.176*	0.148	0.0582	0.0236	0.007 29	0.002 08					
375	10.8	10.5	7.65	1.01	0.145	0.0306	0.0112*	0.006 06	0.123	0.0370	0.0337	0.0265	0.0191*	0.005 39	0.002 48					
500	9.6	9.78	7.55	0.776	0.114	0.0198	0.0152	0.004 59	0.0690	0.0122	0.0188	0.0193	0.0118	0.005 85	0.001 31					

TABLE IV. Absolute cross sections (in units of 10^{-16} cm^2) for He^{2+}-Kr collisions. Notation and uncertainties are as given for Table I.

	He^{2+}-Kr																									
E/M	Direct ionization											Single capture										Double capture				
(keV/u)	σ_+	σ_-	σ_1^{22}	σ_2^{22}	σ_3^{22}	σ_4^{22}	σ_5^{22}	σ_6^{22}	σ_7^{22}	σ_8^{22}	σ^{21}	σ_1^{21}	σ_2^{21}	σ_3^{21}	σ_4^{21}	σ_5^{21}	σ_6^{21}	σ_7^{21}	σ_8^{21}	σ^{20}	σ_2^{20}	σ_3^{20}	σ_4^{20}	σ_5^{20}	σ_6^{20}
5	35	6.71									22.9	18.5	4.01	0.375	0.0459					2.66	0.895	1.69	0.0620		
10	39	8.71									23.4	18.9	4.40	0.557	0.172	0.0131				3.45	1.18	1.96	0.313	0.0139	
16.7	39.7	10.9	1.37*	0.0566							21.9	17.5	2.93	1.28*	0.264*	0.0283				3.48	1.10	1.80	0.534	0.0442	
33.3	36.5	15.8	4.69	0.333	0.0845	0.0369					15.7	10.5	3.34	1.46	0.349	0.0625	0.007 59			2.52	0.802	1.11	0.496	0.109	0.009 31
50	33	19.1	7.22	0.853	0.203	0.0425					11.2	6.07	3.10	1.46	0.432	0.0762	0.0106			1.36	0.356	0.610	0.311	0.0725	0.012 1
66.7	30	20.0	8.84	1.11	0.305	0.0529					8.46	3.93	2.70	1.37	0.363	0.0779	0.0156			0.754	0.199	0.336	0.161	0.0514	0.007 22
50	33	18.5	8.03	0.827	0.147	0.0190*					11.0	6.38	2.84	1.27	0.346	0.0954	0.0141*			1.38*	0.747*	0.610	0.261	0.0809	0.0140*
75	29.0	22.4	11.3	1.49	0.340	0.0465*					7.64	3.61	2.43	1.16	0.322*	0.103	0.0186	0.001 21		0.786	0.353*	0.275*	0.108	0.0409	0.009 69*
100	26.0	20.6	10.4	1.66	0.397	0.0521*	0.0164*	0.009 71			5.72	2.52*	1.92	0.921	0.250	0.0914	0.0218*	0.004 75		0.339*	0.164*	0.0999*	0.0433*	0.0253	0.006 1
175	21.5	21.7	12.6	2.45	0.551	0.118	0.0491*	0.0128			1.77	0.499*	0.450*	0.257*	0.118	0.0502	0.0190	0.005 65	0.001 36	0.0258*	0.009 55*	0.006 62*	0.004 44*	0.004 02*	0.002 29
250	17.8	16.4	10.2	1.70	0.391	0.105	0.0570*	0.0173*	0.003 38		0.477	0.130	0.117*	0.119	0.0623*	0.0385	0.0151	0.003 08*	0.001 27						
375	14.5	13.1	8.73	1.08	0.286	0.0925	0.0616*	0.0162*	0.007 88	0.001 43	0.246	0.0305	0.0478	.0729	0.0508*	0.0271*	0.0114*	0.003 72*	0.002 11						
500	12.4	12.6	8.79	0.870	0.261	0.0910	0.0627	0.0203*	0.0106	0.0034	0.170	0.0159*	0.0353*	0.0526	0.0318	0.0214	0.008 25	0.003 52*	0.001 06						

gle ionization is roughly independent of impact energy.

At the other extreme is the possibility for the projectile to interact with each target electron independently in order to ionize them. This "multistep" independent-electron interaction implies that the qth-order ionization cross section should behave as the qth power of the single-ionization cross section.

This can easily be shown by assuming an independent-electron binary encounter approach to the ionization of q electrons from a shell containing N electrons. Doing so yields

$$\sigma_q^{ii}=2\pi\int_0^\infty \binom{N}{q} P(b)^q[1-P(b)]^{N-q}bdb \ .$$

If, for simplicity, an ionization probability that decreases exponentially as a function of impact parameter is assumed [i.e., $P(b)=P(0)e^{-b/R}$ where R is a characteristic interaction distance roughly corresponding to the shell diameter], the direct-multiple-ionization cross sections are given by

$$\sigma_q^{ii}=\frac{2\pi R^2}{q^2}\binom{N}{q}P(0)^q\approx(\sigma_1^{ii})^q \ .$$

Thus where a multistep interaction dominates, σ_q^{ii} should be proportional to $(\sigma_1^{ii})^q$. This is in contrast to the single-step interaction that dominates at high impact energies where the σ_q^{ii} is proportional to σ_1^{ii}.

In order to test whether the multistep-interaction mechanism is important, the above equations can be solved for R in terms of the ionization cross sections σ_q^{ii}. Doing so yields

$$R=\left[\frac{2\pi}{q^2}\frac{1}{(2\pi N)^q}\binom{N}{q}\frac{(\sigma_1^{ii})^q}{\sigma_q^{ii}}\right]^{1/(2q-2)} .$$

Where the multistep-interaction mechanism dominates, this simple model predicts that R will have only a weak impact energy dependence. This is because $\sigma_q^{ii}\approx(\sigma_1^{ii})^q$. For example, a detailed theoretical analysis[1] predicts that single ionization should behave as $v^{-2}\ln(v)$ for large impact velocities v whereas double ionization should have a v^{-4} dependence. Thus, where the multistep-interaction mechanism dominates, R is expected to increase slowly with increasing impact energy. This is in contrast to the single-step interaction which predicts that $\sigma_q^{ii}\approx\sigma_1^{ii}$ and hence the ratio $\sigma_q^{ii}/\sigma_1^{ii}$ is expected to be energy independent.

Values of R have been calculated for He^{2+} impact on helium using the tabulated data presented above in order to determine whether a single interaction or a multistep interaction dominates in the energy range investigated. The results, along with results obtained for other fully stripped ion impact, are shown in Fig. 5. Previously[4] it was shown that for proton impact a nearly constant R occurs in the range 50–500 keV (solid curve in Fig. 5) whereas a constant $\sigma_2^{ii}/\sigma_1^{ii}$ was found[1] only for energies larger than approximately 5 MeV. This was interpreted to mean that between 50 and 500 keV *only* a multistep interaction is important in leading to direct double ionization of helium, above 5 MeV only the single-step interaction is important, and for intermediate energies both contribute. It is possible that the emerging influence of the single-step mechanism at the higher impact energies is disguising the expected slow energy dependence of R.

The He^{2+} data indicates that again the multistep-interaction mechanism as described above is dominant in the production of doubly ionized helium. Not only is R nearly constant found but it is the *same* value as was found for proton impact. In fact, *all* the bare-ion data are found to lie on the same curve. Also note that R for fully stripped ions other than protons may be slowly increasing at the higher impact energies as is predicted

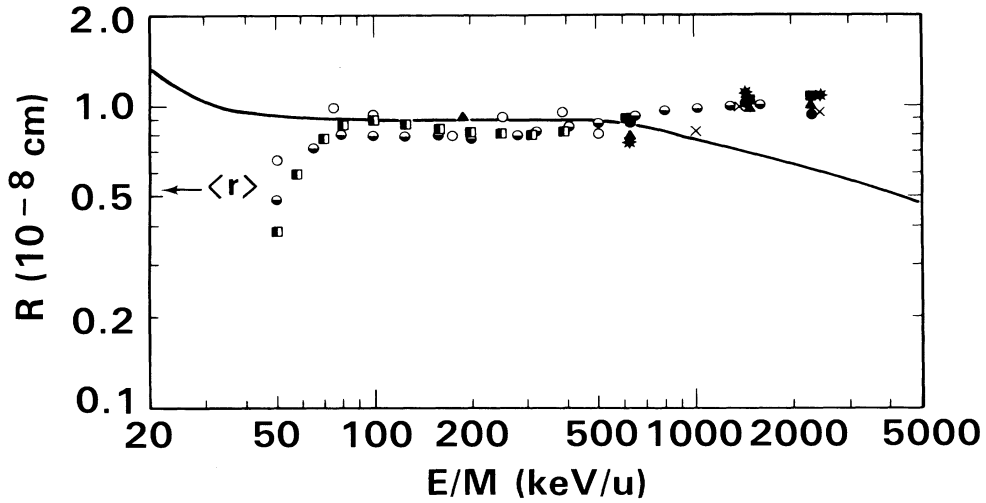

FIG. 5. Interaction distance obtained from the independent electron analysis described in text. H^+ impact: ——, Ref. 4. He^{2+}: ○, present work; ◒, Ref. 2. Li^{3+}: ◧, Ref. 2; ■, Ref. 3. B^{5+}: ▲, Ref. 3. C^{6+}: ⁎, Ref. 3. O^{8+}: ×, Ref. 3. $\langle r\rangle$ is the mean radius of the helium 1s electron.

TABLE V. Relative values of the detection efficiencies for slow target ions taken from Fig. 2(a). See Appendix for details.

Target-ion charge state	Target ion detection efficiencies $\eta(q)$						
q	He	Ne	Ar	Kr	Li	Na	Mg
1	0.88	0.50	0.33	0.17	0.80	0.53	0.52
2	0.91	0.67	0.51	0.33	0.90	0.70	0.69
3		0.76	0.60	0.42		0.78	0.77
4			0.67	0.50		0.82	0.83
5			0.72	0.53			

theoretically.[1] However, the major point to be derived from the data is that the multistep interaction leading to double ionization of helium is essentially the same for all fully stripped ions. The only difference is the extent to which the multistep interaction dominates the single-step interaction at higher velocities.

A similar analysis using the small amount of neon data that is available leads to exactly the same conclusions. Argon and krypton were not analyzed since in these cases it is essential to separate outer-, from inner-, shell ionization[4] and insufficient information currently exists to do so.

V. SUMMARY

Data for multiple ionization of helium, neon, argon, and krypton by bare helium ions have been presented. The present data have been combined with recalculated cross sections that were published earlier in order to provide a complete picture of ionization between 5 and 500 keV/amu. The earlier measurements which indicated that double capture plus an additional ionization were more probable than pure double capture from argon and krypton were shown to be in error due to inaccurate recoil-ion detection efficiencies previously assumed. When compared to the previous total cross-section measurements of Itoh and Rudd, it was found that the present data yield smaller free-electron-production cross sections at low impact energies and slightly larger capture cross sections.

By analyzing the direct-multiple-ionization cross sections for helium and neon, it was shown that these data can be well represented by an independent-electron, multiple projectile-target interaction model. For the helium target all available data for bare-ion impact were shown to conform with this model over a broad range of impact velocities.

ACKNOWLEDGMENT

This work was supported by the Office of health and Environmental Research (OHER), U.S. Department of Energy under Contract No. DE-AC06-76RLO 1830.

APPENDIX

The multiple-ionization cross sections previously presented in Refs. 5 and 9–11 are in error due to inaccurate information available at that time regarding the detection efficiencies for the slow target ions. These efficiencies were previously taken to be unity for all recoil-ion charge states. The correct values, taken from Fig. 2(a) of this paper, are seen in Table V. Using these detection efficiencies, the correct values for the σ_q^{ij} cross sections can then be obtained from the values previously presented $(\sigma_q^{ij})^*$ by

$$\sigma_q^{ij}=\frac{(\sigma_q^{ij})^*\sigma^{i,i-1}}{\eta(q)\sum[(\sigma_q^{i,i-1})^*/\eta(q)]} .$$

This will result in only small changes for the lighter targets with larger corrections required for the heavier targets.

[1] J. H. McGuire, Phys. Rev. Lett. **49**, 1153 (1982); J. Phys. B. **17**, L779 (1984).
[2] M. B. Shah and H. B. Gilbody, J. Phys. B **18**, 899 (1985).
[3] H. Knudsen, L. H. Andersen, P. Hvelplund, G. Astner, H. Cederquist, H. Danared, L. Liljeby, and K.-G. Rensfeld, J. Phys. B **17**, 3545 (1984).
[4] R. D. DuBois and S. T. Manson, Phys. Rev. A **35**, 2007 (1987).
[5] R. D. DuBois, Phys. Rev. A **33**, 1595 (1986).
[6] R. L. Becker, A. L. Ford, and J. F. Reading, Second International Seminar on High-Energy Ion-Atom Collisions, Debrecen, 1984 (unpublished); Proceedings of the Eighth International Conference on the Application of Accelerators in Research and Industry, Denton, Texas, 1984, edited by J. L. Duggan, I. L. Morgan, and J. A. Martin [Nucl. Instrum. Methods B **10/11**, 1 (1985)].
[7] A. Itoh and M. E. Rudd, Phys. Rev. A **32**, 2128 (1985).
[8] J. Fricke, A. Müller, and E. Salzborn, Nucl. Instrum. Methods **175**, 379 (1980).
[9] R. D. DuBois, Phys. Rev. Lett. **52**, 2348 (1984).
[10] R. D. DuBois, Phys. Rev. A **32**, 3319 (1984).
[11] R. D. DuBois, Phys. Rev. A **34**, 2738 (1986).
[12] L. J. Puckett, G. O. Taylor, and D. W. Martin, Phys. Rev. **178**, 271 (1969).
[13] C. F. Barnett, J. A. Ray, E. Ricci, M. I. Wilker, E. W. McDaniel, E. W. Thomas, and H. B. Gilbody, Oak Ridge National Laboratory Publication No. ORNL-5206, 1977 (unpublished), Vol. 1.
[14] M. E. Rudd, R. D. DuBois, L. H. Toburen, C. A. Ratcliffe, and T. V. Goffe, Phys. Rev. A **28**, 3244 (1983).
[15] Y. Nakai, A. Kikuchi, T. Sharai, and M. Sataka, Japan Atomic Energy Research Institute Publication No. JAERI-M 84-069, 1984 (unpublished).